Magnetic structure and enhanced T_N of the rare-earth intermetallic compound $TbRhIn_5$: Experiments and mean-field model

R. Lora-Serrano,[1,*] C. Giles,[1] E. Granado,[1,2] D. J. Garcia,[1] E. Miranda,[1] O. Agüero,[1] L. Mendonça Ferreira,[1] J. G. S. Duque,[1] and P. G. Pagliuso[1]

[1]*Instituto de Física "Gleb Wataghin," UNICAMP, 13083-970, Campinas, São Paulo, Brazil*

[2]*Laboratório Nacional de Luz Síncrotron, Caixa Postal 6192, CEP 13084-971 Campinas, São Paulo, Brazil*

(Received 21 February 2006; revised manuscript received 1 October 2006; published 4 December 2006)

In this work the physical properties of the intermetallic compound $TbRhIn_5$ were investigated by means of temperature-dependent magnetic susceptibility, electrical resistivity, heat-capacity, and resonant x-ray magnetic diffraction experiments. $TbRhIn_5$ is an intermetallic compound that orders antiferromagnetically at T_N=45.5 K, the highest ordering temperature among the existing RRhIn$_5$ (1-1-5, R=rare earth) materials, which in contrast to what is expected from a de Gennes scaling along the RRhIn$_5$ series. The x-ray resonant diffraction data have allowed us to solve the magnetic structure of $TbRhIn_5$. Below T_N, we found a commensurate antiferromagnetic structure with a propagation vector $(1/2,0,1/2)$ and the Tb moments oriented along the c axis. Strong (over two orders of magnitude) dipolar enhancements of the magnetic Bragg peaks were observed at both Tb absorption edges L_{II} and L_{III}, indicating a fairly high polarization of the Tb $5d$ levels. Using a mean-field model including an isotropic first-neighbor exchange interaction ($J_{R\text{-}R}$) and the tetragonal crystalline electrical field (CEF), we evaluate the influence of the CEF effects in the physical properties of $TbRhIn_5$. The results reported here seem to corroborate a general trend of CEF-driven effects on T_N along the RRhIn$_5$ series.

DOI: 10.1103/PhysRevB.74.214404 PACS number(s): 75.50.Ee, 75.25.+z, 74.70.Tx, 75.10.Dg

I. INTRODUCTION

The discovery of new series of structurally related compounds with novel physical behavior is an important approach to explore fundamental problems in the physics of highly correlated electron systems. Such problems include the interplay between superconductivity, magnetism, and heavy-fermion behavior in structurally related materials.[1,2] Although the microscopic origin of this interplay remains a mystery, the search for new heavy-fermion superconductors (HFSs) is partially guided by the knowledge that certain structures favor the formation of this heavy electron ground state. Remarkable examples of amazing physical properties occurring in structurally related compounds are the series Ce_mMIn_{3m+2} (M=Co, Rh, or Ir, m=1,2), [3–7] and their Pu-based analogs PuMGa$_5$.[8–10] These materials grow in a tetragonal variant of the Cu_3Au-type structure and can be viewed as layers of a cubic cell ($CeIn_3$ or $PuGa_3$) stacked sequentially along the c axis with intervening layers of $M(In,Ga)_2$.[11] The discovery of unconventional superconductivity (USC) in many of these compounds is an exciting opportunity to further explore the possibility of magnetically mediated superconductivity in strongly correlated electron systems and its relationship with dimensionality and crystal structures. For instance, systematic alloying studies in $CeRh_{1-x}Ir_xIn_5$ (Refs. 12 and 13) and $PuCo_{1-x}Rh_xGa_5$ (Ref. 9) ($PuCoGa_5$ possesses the highest superconducting transition temperature, T_c=18 K, among the pure Pu-based compounds[8]) have revealed an intriguing linear dependence between T_c and the ratio of the tetragonal lattice parameters c/a at ambient pressure, indicating that the increasing of the quasi-two-dimensional (2D) character of their crystal structure may favor USC.

Like the high-T_c and the organic superconductors, HFSs are believed to be magnetically mediated superconductors.[14] Furthermore, in most cases, USC seems to occur at the vicinity of a magnetically ordered state and the spin fluctuations (SFs) associated with this magnetic phase may mediate the superconducting pair formation.[14] More recently, a bridge connecting the HFSs and high-T_c superconductors (HTSCs) has been proposed by NMR studies in $PuCoGa_5$. These studies have shown that superconductivity in this material is unconventional with d-wave symmetry and similar properties to those found in other HFSs and HTSCs, suggesting that these classes of complex USC may share the same pairing mechanism.[10]

Focusing our attention now on the Ce-based HFSs, the magnetic properties of these materials are associated with their $4f$ electrons. Although these compounds display obvious heavy-fermion behavior, evidence for low-temperature $4f$ local moment behavior has also been found in this family.[15–17] This apparent contradiction is directly related to an open question in condensed matter physics regarding the details of the crossover between quasilocalized $4f$ electron magnetic behavior at high T to a renormalized heavy-electron state at lower temperatures. However, if certain structures favor USC mediated by magnetic fluctuations, it is an important first step to understand how layered structures can affect crystalline electric field (CEF) anisotropy, magnetic exchange and/or anisotropic transport properties (quasi-2D band structure). In this regard, detailed studies of the $4f$ electron magnetism along the series of rare-earth- and actinide-based 1-1-5 compounds may be very informative.

In the case of the Ce-based compounds, their Nd-, Sm-, and Gd-based structurally related magnetic materials have been studied in detail.[18–24] It has been found that the magnetic properties of these non-Ce analogs mainly depend on the interplay between CEF effects and exchange magnetic interaction. For example, among the Nd-based compounds

$NdMIn_5$ and Nd_2MIn_8 analogs for M=Rh or Ir, a systematic relationship was found between the antiferromagnetic (AFM) ordering temperature T_N and the low-T CEF splitting.[19] In addition, when the magnetic properties of the tetragonal variants $NdMIn_5$ and Nd_2MIn_8 are compared to that for cubic $NdIn_3$, T_N is enhanced by a factor of 2.[13,19,25] In contrast, the tetragonal $CeRhIn_5$ and Ce_2RhIn_8 present a T_N a factor of 2 smaller than that for $CeIn_3$, whereas for the Gd-based tetragonal materials the low-temperature magnetic properties remain nearly unaltered compared to the $GdIn_3$.[13,19,25] Finally, the resolved magnetic structures for some of these compounds have revealed that the rare-earth magnetic moments lie in the *ab* plane for $CeRhIn_5$ and $GdRhIn_5$ compounds and point along the *c* axis for $NdRhIn_5$ tetragonal materials.[21–24]

To further explore the trends in the evolution of the magnetic properties within the series, particularly for the $RRhIn_5$ compounds, we have investigated in greater detail[25] the physical properties and solved the magnetic structure of $TbRhIn_5$. The enhanced T_N of $TbRhIn_5$ compared to its cubic relatives and/or compared to its counterparts the $RRhIn_5$ series could be explained by the details of the tetragonal CEF of a given rare earth, as previously shown by theoretical calculation using a mean-field model including an isotropic first-neighbors exchange interaction ($J_{R\text{-}R}$) and the tetragonal CEF.[26] Particularly for Tb^{3+} ions, an enhancement of T_N is more likely to occur when the Tb ordered moments are aligned along the *c* axis. Using resonant x-ray magnetic diffraction (XRMS) experiments, we have resolved the magnetic structure of $TbRhIn_5$ and shown that in fact the Tb moments orient along the *c* axis and form a commensurate antiferromagnetic structure with propagation vector $\tau=(\frac{1}{2},0,\frac{1}{2})$. Using the same model of Ref. 26 we have tried to investigate the influence of the CEF effect on the macroscopic properties of $TbRhIn_5$. From simultaneous fits to the anisotropic magnetic and specific-heat data (with the constraint of having the easy axis along the *c* direction) using this model, we extract a preliminary CEF scheme and a set of CEF parameters for $TbRhIn_5$.

Apart from the necessary confirmation of the CEF scheme of $TbRhIn_5$ with additional experiments [for instance by inelastic neutron scattering (INS)], the reported results seem to confirm the CEF-driven T_N behavior and the direction of ordered moments observed in other members of the series. We discuss also the particular case where the rare-earth moments order out of the *c* axis, for which T_N can be reduced by tuning the CEF parameters. This fact represents an interesting frustration mechanism that may play some role in the origin of the relevant low-dimensional SFs in complex classes of materials such as the Ce_mMIn_{3m+2} (M=Rh, Ir, and Co; m=1,2) HFSs.

II. EXPERIMENT

Single crystals of $TbRhIn_5$ with dimensions up to approximately 2 cm^3 were grown from In flux, as reported previously.[3–5] Most of the crystals show columnar habit, with their long axis along the tetragonal *c* axis. The tetragonal $HoCoGa_5$-type structure[11] with cell parameters a=4.595(4) Å and c=7.418(4) Å were confirmed by x-ray powder diffraction and the crystal orientation was determined by the usual Laue method. Specific-heat measurements were performed in a Quantum Design physical properties measurement system (PPMS) small-mass calorimeter that employs a quasiadiabatic thermal relaxation technique. Magnetization measurements were made in a quantum design dc superconducting quantum interference device and electrical resistivity was measured using the PPMS low-frequency ac resistance bridge and four-contact configuration. The samples used in the electrical resistivity were screened to be free of surface contamination by residual In flux.

XRMS measurements were carried out at the bending magnet beamline XRD2 of the Brazilian Synchrotron Light Source (LNLS), in Campinas, Brazil using a double-bounce Si(111) monochromator, with sagittal focusing.[27] A Rh-coated mirror was used to vertically focus the beam and also to eliminate third- and higher-order harmonics in the incident beam. The bending magnet source delivers photon beams with a flux of $\sim 3\times 10^{10}$ photons/s around 8 keV at 100 mA in a spot of area $\sim$0.6 (vertical) $\times$ 2.0 mm^2 (horizontal) at the sample, with an energy resolution from the source of $\delta E/E \sim 10^{-4}$. Our experiments were performed in the vertical scattering plane, i.e., perpendicular to the linear polarization of the incident photons (σ polarization[28]).

A platelet of $TbRhIn_5$, from the same batch as that used for macroscopic property measurements, was mechanically polished perpendicular to the *c* axis [(00l) flat surface] to eliminate surface contamination from the residual flux and to increase the reflectivity, which gives a mosaic spread characterized by the full width at half maximum (FWHM) of $\sim 0.04°$. The sample was cut parallel to the *ab* plane to have the final shape of a long block with dimensions of $4\times 3\times 1$ mm^3 and to investigate reflections in the [*h*0*l*] zone axis. The size of the sample was chosen to ensure that the whole incident beam is intercepted by the c-axis surface for all angles of interest. The sample was mounted on the cold finger of a closed-cycle He cryostat (base temperature 11 K) with a cylindrical Be window.

III. RESULTS

The temperature dependence of the magnetic susceptibility measured for a magnetic field H=1 kOe applied parallel $\chi_\parallel$ and perpendicular $\chi_\perp$ to the *c* axis is presented in Fig. 1(a). Figure 1(b) shows the polycrystalline average of Fig. 1(a) data taken as $\chi_{poly}=(\chi_\parallel+2\chi_\perp)/3$.

From a linear fit to the inverse of $\chi_{poly}(T)$ for $T>140$ K using a Curie-Weiss law, we have obtained a Curie-Weiss temperature $\theta=-47(1)$ K and the Tb^{3+} effective magnetic moment $\mu_{eff}=9.4(1)\mu_B$. As can be seen in Fig. 1(a) the magnetic susceptibility of $TbRhIn_5$ is higher for the field applied along the *c* axis, in agreement to what was found for all other R members except Gd.[3,18,19] The ratio $\chi_\parallel/\chi_\perp \sim 2.08$ taken at T_N is mainly determined by the tetragonal CEF and it reflects the same order of magnetic anisotropy found for other members of these series.[3,18,19] The solid lines in Fig. 1(a) are the best fits to the data using the mean-field model of Ref. 26.

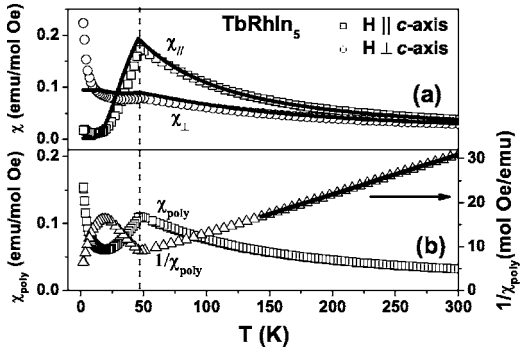

FIG. 1. (a) Temperature dependence of the magnetic susceptibility for $TbRhIn_5$, for $H=1$ kOe applied parallel ($\chi_{\|}$) (open squares) and perpendicular to the c axis ($\chi_{\perp}$) (open circles). The solid lines are best fits to the data for both directions using our mean-field model (see below). (b) $\chi_{poly}(T)$ and the inverse $1/\chi_{poly}(T)$; the solid line is the linear fit to the $1/\chi_{poly}$ data for $T>140$ K. From this fit we extracted $\mu_{eff}=9.4(1)\mu_B$ and $\theta=-47(1)$ K for $TbRhIn_5$.

The best fit yields a $J_{R\text{-}R}=0.2$ meV ($J_{R\text{-}R}$ is equal to zK_{RKKY} in the notation of Ref. 26) for the exchange parameter and the CEF parameters $B_{20}=-1.4\times10^{-1}$ meV, $B_{40}=1.3\times10^{-4}$ meV, $B_{44}=-5.3\times10^{-3}$ meV, $B_{60}=0.21\times10^{-4}$ meV, and $B_{64}=1.5\times10^{-4}$ meV. The CEF level scheme obtained from the splitting of the Tb^{3+} ($J=6$) multiplet in the tetragonal symmetry, given by the above parameters, is built up of three doublets (where the lowest energy level is represented by the $\Gamma_5^{(1)}$ doublet; see Table I and seven singlets with an overall splitting of roughly 310 K. The energies and wave functions of each particular CEF state are given in Table I.

It is important to point out that the obtained CEF scheme and the set of parameters need confirmation by further experiments such as INS. Particularly for low-symmetry systems like $TbRhIn_5$, a meticulous and systematic analysis of a large set of experiments including INS may be required to unambiguously obtain a CEF scheme and a unique set of CEF parameters.[29–31]

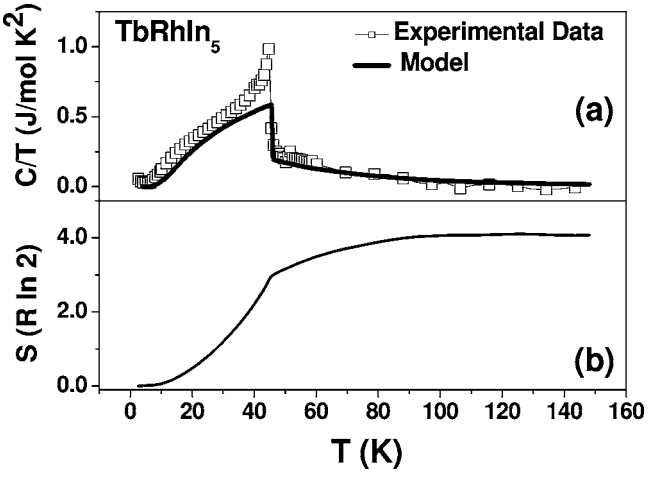

FIG. 2. (a) Specific-heat data divided by temperature as a function of temperature for a single crystal of $TbRhIn_5$. The solid line is the best fit to these data using our mean-field model. (b) The corresponding magnetic entropy in the temperature range $2<T<150$ K for $TbRhIn_5$.

TABLE I. CEF states and associated energies E_i and eigenfunctions Ψ_i for Tb^{3+} ion ($J=6$) in tetragonal symmetry according to results from the mean field-model.

Label Γ_i	E_i (K)	Eigenfunctions Ψ_i
$\Gamma_5^{(1)}$	0	$-0.99\|\pm5\rangle+0.042\|\pm1\rangle+0.132\|\mp3\rangle$
$\Gamma_3^{(2)}$	65	$-0.843\frac{(\|6\rangle+\|-6\rangle)}{\sqrt{2}}+0.537\frac{(\|2\rangle+\|-2\rangle)}{\sqrt{2}}$
$\Gamma_4^{(2)}$	84	$-0.983\frac{(\|6\rangle-\|-6\rangle)}{\sqrt{2}}+0.18\frac{(\|2\rangle-\|-2\rangle)}{\sqrt{2}}$
$\Gamma_1^{(1)}$	100	$0.724\frac{(\|-4\rangle+\|4\rangle)}{\sqrt{2}}+0.689\|0\rangle$
$\Gamma_5^{(2)}$	122	$-0.132\|\pm5\rangle-0.817\|\pm1\rangle-0.561\|\mp3\rangle$
Γ_2	137	$\frac{(\|-4\rangle-\|4\rangle)}{\sqrt{2}}$
$\Gamma_3^{(1)}$	155	$0.537\frac{(\|6\rangle+\|-6\rangle)}{\sqrt{2}}+0.843\frac{(\|2\rangle+\|-2\rangle)}{\sqrt{2}}$
$\Gamma_1^{(2)}$	179	$-0.689\frac{(\|-4\rangle+\|4\rangle)}{\sqrt{2}}+0.724\|0\rangle$
$\Gamma_5^{(3)}$	274	$-0.04\|\pm5\rangle+0.826\|\pm1\rangle-0.562\|\mp3\rangle$
$\Gamma_4^{(1)}$	310	$0.18\frac{(\|6\rangle-\|-6\rangle)}{\sqrt{2}}+0.983\frac{(\|2\rangle-\|-2\rangle)}{\sqrt{2}}$

As a preliminary analysis, our model with the set of parameters above could reproduce well the magnetic anisotropy and the peak of the magnetic susceptibility at $T_N\sim45.5$ K for both directions [Fig. 1(a)]. At lower T an anisotropic Curie-like tail was found in the magnetic susceptibility data for all measured crystals. We could not reproduce simultaneously the high-T anisotropy, the peak at T_N, and the low-T tails for any set of parameters. Further experiments at lower T are needed to establish the origin of this behavior.

Figure 2(a) shows the specific heat divided by temperature and the corresponding magnetic entropy [Fig. 2(b)] in the temperature range $0<T<150$ K for $TbRhIn_5$. To calculate the magnetic entropy, the phonon contribution was estimated from the nonmagnetic specific-heat data of $YRhIn_5$ and subtracted from the total specific heat of the magnetic compound. The recovery magnetic entropy at high T is close to its expected values for $J=6$. An anomaly in the specific-heat data associated with the onset of AFM order can be seen at $T_N=45.5$ K in good agreement with the temperatures where the maximum in the magnetic susceptibility occurs (see Fig. 1). Again, the solid line in Fig. 2(a) represents the best fit to the data using our model for the same parameters

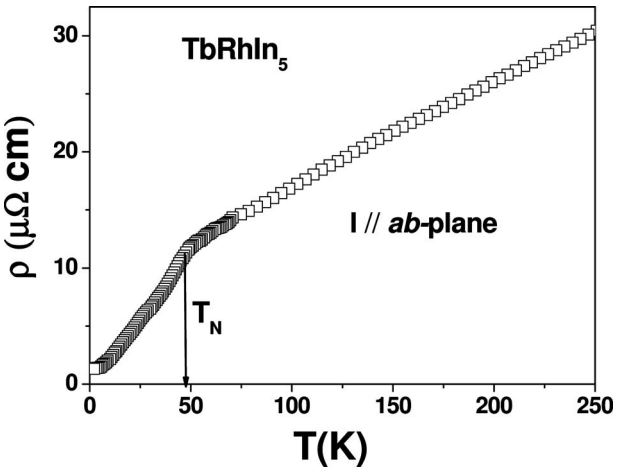

FIG. 3. Temperature dependence of the electrical resistivity for $TbRhIn_5$ single crystal. The current (I) has been applied parallel to the ab plane. The solid arrow points out a kink at the Néel temperature for this compound.

used in the fit of the $\chi(T)$ data [the best set of parameters was obtained from simultaneous minimization process for both $\chi(T)$ and $C/T(T)$ data]. It is evident that a reasonable agreement between the experimental data and the fits is also obtained for the heat capacity data with the exception of the $T \approx T_N$ temperature range where the contribution of magnetic fluctuations are important.

The temperature dependence of the electrical resistivity for $TbRhIn_5$ single crystals is plotted in Fig. 3. Among various measured crystals, the room temperature value of the resistivity ranges between 10 and 35 $\mu\Omega$ cm. At high temperature the data always showed a metallic behavior while, at low temperatures, a clear kink can be seen at the ordering temperature T_N.

The c/a ratio and T_N values for $R\mathrm{RhIn}_5$ compounds are shown in Fig. 4. The solid line in Fig. 4(a) is the expected behavior for T_N and θ according to the de Gennes factor $(g_J-1)^2J(J+1)$ for the ground-state multiplet J of each rare earth normalized by its value for $GdRhIn_5$. As for R=Ce and

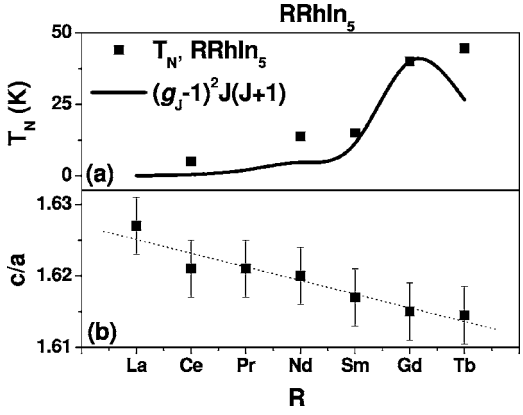

FIG. 4. T_N (a) and c/a ratio (b) for the $R\mathrm{RhIn}_5$ compounds. The solid line in (a) represents the de Gennes factor $(g_J-1)^2J(J+1)$ for the ground-state multiplet J of the rare-earth ions, normalized by $GdRhIn_5$. The dashed line in (b) is just a guide to the eye.

Nd,[19] T_N of $TbRhIn_5$ does not follow the de Gennes scaling. Interestingly, T_N for $TbRhIn_5$ is the highest among the existing $R\mathrm{RhIn}_5$ members.

The microscopic low-temperature magnetism of $TbRhIn_5$ was further investigated by XRMS. For the sample orientation used in the experiments, with the zone axis $[h0l]$ parallel to the scattering plane, the resonant scattering cross section (the nonresonant scattering contribution was observed to be negligible) for the case of a dipolar resonance with a linear polarized incident beam perpendicular to the scattering plane may be written as[28,32]

$$I \propto \left| \sum_n \hat{u}_n \cdot \hat{k}_f e^{i\mathbf{Q}\cdot\mathbf{r}_n} \right|^2 \tag{1}$$

where $\mathbf{Q}=\mathbf{k}_f-\mathbf{k}_i$ is the scattering vector, $\hat{k}_f$ is the direction of the scattered wave vector $\mathbf{k}_f$, and $\hat{u}_n$ is the moment direction at the nth site. The proportionality symbol includes $\mathbf{Q}$-independent resonant amplitudes, the Lorentz factor, arbitrary scale factors, and an angular correction factor for asymmetric reflections. The summation is over all the nth resonant ions in the magnetic unit cell and $\mathbf{r}_n$ is the position of such an ion. Note that in the present geometry and in the absence of an in-plane π-polarized component of the incident beam, the dipolar resonant cross section terms are not sensitive to the component of the ordered moment perpendicular to the scattering plane (i.e., along the b axis).

Below $T_N \sim 46$ K, careful scans along the $[h0l]$ direction revealed superstructure Bragg peaks of type $(\frac{2n+1}{2},0,\frac{2m+1}{2})$ (n, m integers), appearing as a result of the strong resonant enhancements of the magnetic peaks for both Tb L_{II} and L_{III} edges, and the high magnetic moment per Tb^{3+} ion of $\mu=9.5\mu_B$. In the low-temperature phase, magnetic peaks $(0,\frac{2n+1}{2},\frac{2m+1}{2})$ were also observed, revealing a twinned magnetic structure. The intensities of $(\frac{2n+1}{2},0,\frac{2m+1}{2})$ and $(0,\frac{2n+1}{2},\frac{2m+1}{2})$ were comparable, suggesting approximately equal domain population. Therefore, our magnetic cell is duplicated in the a and c directions when compared to the chemical one. Above T_N only charge peaks consistent with the tetragonal $HoCoGa_5$-type structure were observed. The widths (FWHM) of magnetic peaks were the same as that for equivalent scans through a charge Bragg peak.

The magnetic structure of $TbRhIn_5$ was then resolved from the obtained modulation vector $\tau=(\frac{1}{2},0,\frac{1}{2})$ and the magnetic moment direction was established by comparing the observed intensities of some magnetic Bragg reflections with a model based on the resonant cross section of Eq. (1) (this method was first used in Ref. 33, where the reader can find more details about the correction factors entering the proportionality symbol). In Fig. 5, the integrated intensities of five magnetic reflections obtained at T=20 K are shown as solid squares. We used asymmetric reflections ($\mathbf{Q}$ vector out of the scattering plane) of the type $(0,\frac{2n+1}{2},\frac{2m+1}{2})$ in order to also analyze the b-axis component in the resonant cross section, which cannot be distinguished with $\mathbf{Q}$ vectors going into the scattering plane [i.e., with $(\frac{2n+1}{2},0,\frac{2m+1}{2})$ reflections]. Experimental reflections were taken at the maximum enhancement of the magnetic signal at the L_{II} edge,

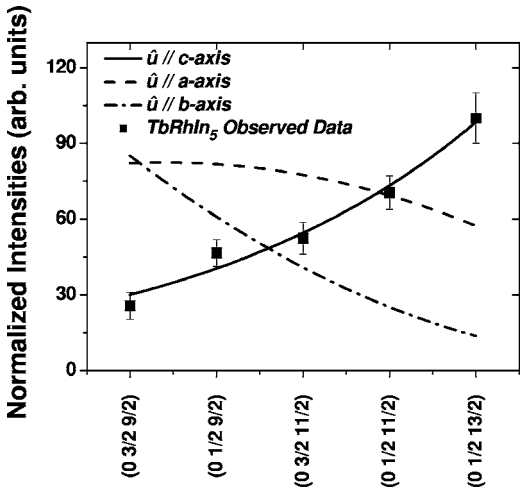

FIG. 5. Integrated intensities of five experimentally obtained magnetic reflections for $TbRhIn_5$ (■) along with calculated intensities for a magnetic moment parallel to the c (solid line), a (dashed line), and b (dash-dotted line) axis. The reliability factor $R=\Sigma_i|I_i^{obs}-I_i^{calc}|/\Sigma_i I_i^{obs}$ is 4.4%.

$E=8253$ eV, and the data have been numerically integrated using Gaussian fit functions (solid squares in Fig. 5).

The comparison between the observed and calculated intensities has been made assuming the Tb^{3+} magnetic moment direction along all directions in the 3D space. The results for three possibilities are shown, the first one assuming the moments along the c direction (solid line), the second with the moments aligned along the a direction (dashed line), and the third one with the moments along the b direction (dash-dotted line). As can be seen in Fig. 5 the model with the ordered moments $\hat{u}\|c$ direction is the one in agreement with the observed data, as suggested by the susceptibility measurements in Fig. 1. A similar trend was also observed for $NdRhIn_5$ family compound[24] in its low-temperature AFM phase with the moment locked in the c axis. Given the experimental errors, the directions of the ordered moments is determined within ~10° of the c direction.

In Fig. 6 the magnetic unit cell of $TbRhIn_5$ is shown according to results depicted in Fig. 5. A half magnetic cell is shown with moment directions at the Tb^{3+} ion crystallographic sites.

In order to use the resonant enhancement of the magnetic peaks, the primary beam energy was tuned to the L_{II} and L_{III} absorption edges of Tb^{3+} ion (tabulated as being 8252 and 7514 eV, respectively). In Figs. 7(a) and 7(b) we plot the scattered intensity of the $(\frac{1}{2},0,\frac{11}{2})$ magnetic Bragg peak as a function of the incident photon energy on tuning through the L_{II} and L_{III} edges, respectively. The data were corrected for absorption [coefficient $\mu(E)$ is shown with the solid line curve and the right side scale in Fig. 7] using the fluorescence emission.[34] The inflection points of $\mu(E)$ curves (vertical dashed line) were used to define the absorption edges. In both cases, the maximum resonant enhancement is observed ~2 eV above the edges, which is a signature of the electric dipole ($E1$) resonance involving electronic transitions $2p_{1/2}\leftrightarrow 5d$ and $2p_{3/2}\leftrightarrow 5d$. A remarkable enhancement of over two orders of magnitude for both edges has been

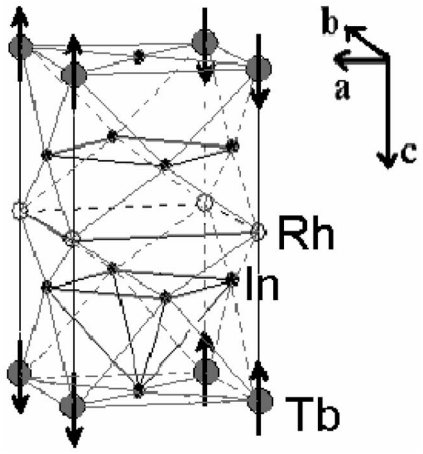

FIG. 6. The magnetic structure of $TbRhIn_5$ at 20 K. A half magnetic unit cell is shown. ↑ (↓) represents the directions "up" ("down") of magnetic moments of Tb (depicted by gray filled circles) along the c axis.

obtained. From the fit to a Lorentzian-squared line profile, the width of resonance were found at both edges as being 6.2 and 6.4 eV for L_{II} and L_{III}, respectively (corrected for energy resolution).

The relative strength $I(L_{III})/I(L_{II})$ of the resonant enhancements (the "branching ratio") of the $E1$ resonances is ~2.9 which is in agreement with the theoretical expectations

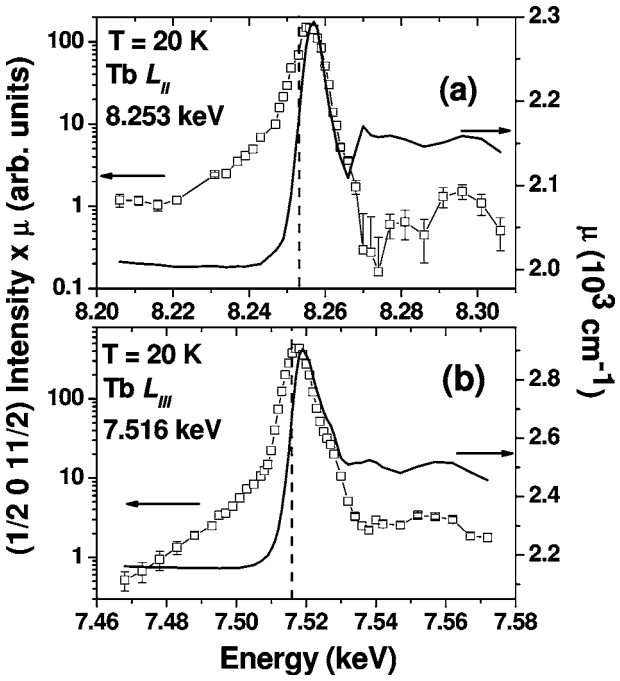

FIG. 7. Energy dependence of the (1/2, 0, 11/2) magnetic peak (open squares) through the Tb L_{II} (a) and L_{III} (b) edges. The open symbols are Gaussian fits to the elastic peak at each energy used in the scan. The data have been corrected for absorption. Solid line curve represents $\mu(E)$ obtained from the fluorescent yield (scale on the right). From the $\mu(E)$ inflection points we determine the absorption edge values (vertical dashed line) as being 8253 eV (L_{II}) and 7516 eV (L_{III}).

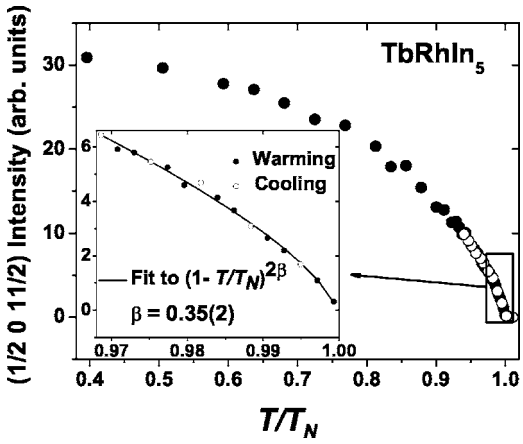

FIG. 8. Temperature dependence of the magnetic Bragg integrated intensities for (1/2, 0, 11/2) magnetic peak. The inset shows in detail the critical region around the transition at the Néel temperature for this compound. From a power-law fit to these data within the temperature range of approximately 3% below T_N we obtain T_N=45.56(2) K and a critical parameter β=0.35(2).

for branching ratios at the rare-earth L edges. This ratio is of interest since it relates to the underlying electronic and magnetic structures (see Refs. 35 and 36, and more recently, Ref. 37 and the references cited therein for more details). According to Ref. 35 in heavy rare-earth elements such as Tb, the $E1$ resonance at the L_{III} is ~2.5 times that of the L_{II} edge and Ref. 37 found a ratio of ~2. These expectations are in agreement with our observations. Intensity oscillations have been observed above the edges, and can be ascribed to magnetic diffraction anomalous fine structure oscillations[38] which are oscillations of the anomalous scattering factors associated with the interference of the photoelectron wave function with the surrounding atoms which cause a fine structure of oscillations in the energy line-shape spectrum.

The behavior of the ordered phase was measured as the temperature was raised at the L_{II} edge. The measurements of the integrated intensities were performed on the $(\frac{1}{2},0,\frac{11}{2})$ satellite reflection. In Fig. 8 the data of longitudinal scans along this reflection are displayed as a function of the reduced temperature T/T_N. As the temperature increases, the peak intensity gradually decreases and disappears above T_N. This result, as well as the one obtained for the energy dependence described above, clearly confirms the magnetic nature of the observed peaks. Data were taken on two regimes: on warming (filled circles in Fig. 8) and cooling (open circles). A fitting to the usual power-law expression $[\sim(1-T/T_N)^{2\beta}]$ for a second-order phase transition (denoted by a solid line in the inset) within the temperature range of approximately 3% below T_N on the warming regime data gives a magnetic transition temperature T_N=45.56(2) K and a critical order exponent β=0.35(2) for the Tb sublattice magnetization. This value of β is compatible with a three-dimensional Heisenberg system. No hysteresis was observed around the ordering temperature and the smooth decrease in intensity in the crossover to the paramagnetic phase is consistent with a second-order transition.

In Table II we summarize the experimental and CEF parameters obtained for $TbRhIn_5$ in this work.

IV. DISCUSSION

As discussed in the Introduction, to follow the evolution of the $4f$ magnetism along the R_mMIn_{3m+2} series is a crucial first step to achieve a deeper understanding of the complex physical properties of these materials. Early comparative studies of the magnetic properties in this family have shown that for the Ce-based materials where the magnetic ordered moments are not aligned along the c axis,[24] T_N is suppressed to less than 0.5 of the $CeIn_3$ value for $CeRhIn_5$ where the Ce magnetic moments lie in the ab plane within the AFM state. On the other hand, for $NdRhIn_5$, where the ordered moments point along the c axis,[24] T_N is significantly enhanced when compared to that for the cubic $NdIn_3$ parent compound. And last, for the Gd-based materials, where the CEF effects are small, the low-temperature magnetic properties remain nearly unaltered compared to those of $GdIn_3$,[13,19,21] suggesting that the low-temperature CEF scheme configuration plays a fundamental role in the observed trends.

Regarding the influence of a given CEF scheme in the AFM ordering temperature, it is reasonable to assume that if a system orders in a given direction and CEF parameters are modified making it more magnetically susceptible in some other direction, but without actually changing the order, the system may experiment some kind of magnetic frustration or the energy barrier between these states should diminish.[26] Therefore, the ordering temperature should decrease as well. Inversely, if the system orders in a certain direction and CEF parameters change favoring even more this state, the ordering temperature should increase.

$TbRhIn_5$ orders antiferromagnetically at T_N=45.5 K, which is an enhanced ordering temperature when compared to T_N~32 K of $TbIn_3$. As $TbRhIn_5$ is more magnetically susceptible for a field applied along the c axis, according to the scenario above, the Tb moment must be ordered along the c axis to explain the enhanced T_N of $TbRhIn_5$.[26]

Taking advantage of the higher **Q** resolution available with x-ray scattering techniques and using the XRMS cross section to determine moment directions in magnetic compounds,[28,33,39] we resolved the magnetic structure of $TbRhIn_5$. Recently, this technique has also been successfully used to determine the magnetic structure of two Gd members of the R_mMIn_{3m+2} (m=1,2; M=Rh,Ir; n=1) series.[20,21]

TABLE II. Experimental and CEF model parameters for $TbRhIn_5$.

a (Å)	c (Å)	T_N (K)	$J_{R\text{-}R}$ (meV)	$\frac{T_{N,RRhIn_5}}{T_{N,RIn_3}}$	B_{20} (meV)	B_{40} (meV)	B_{44} (meV)	B_{60} (meV)	B_{64} (meV)
4.595(4)	7.418(4)	45.5	0.2	1.39	-1.4×10^{-1}	1.3×10^{-4}	-5.3×10^{-3}	0.2×10^{-4}	1.5×10^{-4}

As expected from the idea above, the solved magnetic structure of $TbRhIn_5$ reveals a commensurate AFM structure with propagation vector $(\frac{1}{2},0,\frac{1}{2})$ and the Tb moments oriented along the c axis (see Fig. 6). The direction of the ordered moments was established by comparing the observed intensities of five magnetic Bragg reflections (Fig. 5) with a model based on the resonant cross section for the case of dipolar resonance with a linear polarized incident beam perpendicular to the scattering plane [Eq. (1)].[33] The model considers the possible orientation of the moments along the three tetragonal axes. In Fig. 5 there is obvious agreement between experimental data and the model when the calculations were done assuming the moments along the c direction (solid line).

In addition, the mean-field model of Ref. 26 has shown that the enhancement of T_N for tetragonal compounds that orders axially is a general trend for tetragonal materials when the CEF parameters tend to increase the fluctuations along the c axis. Using this model we were able to fit our susceptibility and specific-heat data, reproducing all the main features of our data, including the prediction of AFM ordering along the c axis[26] for the CEF and $J_{R\text{-}R}$ parameters given in Table II. Although the CEF parameters of Table II may not be the unique set of this data, it is conclusive that the tetragonal CEF can cause the enhanced T_N of $TbRhIn_5$ since the Tb moments order along the c axis.

Therefore, the magnetic properties of the $TbRhIn_5$ compound are another experimental evidence of these general CEF-induced trends along R_mMIn_{3m+2} ($m=1,2$; $M=Rh,Ir$). As such, with the CEF effects being very important in determining T_N, it is expected that the de Gennes scaling will fail to describe the behavior of T_N along the $RRhIn_5$ series (see Fig. 4).

It is important to note that the model of Ref. 26 has also predicted that, for $J=5/2$ and when the system spin is on the plane (for the Ce case), the Néel temperature approximately decreases when the CEF parameters increase fluctuations on the c axis, which is an effective measure of the system preference to be in the c direction. This prediction is consistent with the fact that the tetragonal $CeRhIn_5$ and Ce_2RhIn_8 present higher magnetic susceptibilities when the magnetic field is applied along the c axis, and T_N a factor of 2 smaller than that for $CeIn_3$. It is obvious that the hybridization and Kondo effects are very important in the case of the Ce-based materials, but it is interesting to note that this CEF-driven magnetic frustration mechanism combined with hybridization could create strong in-plane magnetic fluctuations that can mediate the quasi-2D unconventional superconductivity in these systems. It would be interesting to further test this model for other members of the R_mMIn_{3m+2} series that present a decrease of T_N for tetragonal compounds. Although the effect is only about 20%, the tetragonal Sm-based compounds present smaller T_N values than their cubic relative $SmIn_3$.[19] Therefore, according to the present model, the Sm-ordered moment for these materials should be aligned out of the c axis, most likely in the ab plane.

V. CONCLUSION

In conclusion, we have presented results of magnetic susceptibility, electrical resistivity, heat capacity, and x-ray magnetic diffraction experiments for antiferromagnet $TbRhIn_5$. The solved magnetic structure of $TbRhIn_5$ is commensurate with propagation vector $\tau=(\frac{1}{2},0,\frac{1}{2})$ and the Tb moments oriented along the c axis. The direction of the ordering Tb moments and the enhanced T_N of $TbRhIn_5$ compound is another experimental evidence of a more general CEF-induced trend along the R_mMIn_{3m+2} series ($m=1,2$; $M=Rh,Ir$). Using our mean-field model we evaluated the CEF effects on physical properties of $TbRhIn_5$ and proposed a possible CEF scheme and parameters for $TbRhIn_5$. Finally, based on the observed general CEF-induced T_N trend along the R_mMIn_{3m+2} series ($m=1,2$; $M=Rh,Ir$) we speculated that the particular case where the rare-earth moments ordered out of the c axis and the T_N can be reduced by tuning the CEF parameters could give rise to an interesting frustration mechanism that may be relevant to the physical properties of complex classes of materials such as the Ce_mMIn_{3m+2} ($M=Rh,Ir$, and Co; $m=1,2$) HFSs.

ACKNOWLEDGMENTS

We thank A. O. G. Rodriguez and J. Madureira for helpful and interesting discussions about the magnetic moment orientation model. This work was supported by FAPESP (SP-Brazil) Grants No. 03/09861-7, 04/08798-2, 05/00962-0, and 00/08649-6 and CNPq(Brazil) Grants No. 140613/2002-1, 307668/03, 04/08798-2, and 304466/20003-4. LNLS at Campinas is also acknowledged for beam time at the XRD2 beamline.

*Electronic address: rlora@ifi.unicamp.br

[1] Z. Fisk, J. L. Sarrao, J. L. Smith, and J. D. Thompson, Proc. Natl. Acad. Sci. U.S.A. **92**, 6663 (1995).

[2] T. Moriya and K. Ueda, Rep. Prog. Phys. **66**, 1299 (2003).

[3] H. Hegger, C. Petrovic, E. G. Moshopoulou, M. F. Hundley, J. L. Sarrao, Z. Fisk, and J. D. Thompson, Phys. Rev. Lett. **84**, 4986 (2000).

[4] C. Petrovic, R. Movshovich, M. Jaime, P. G. Pagliuso, M. F. Hundley, J. L. Sarrao, J. D. Thompson, and Z. Fisk, Europhys. Lett. **354–359**, 4986 (2001).

[5] C. Petrovic, P. G. Pagliuso, M. F. Hundley, R. Movshovich, J. L. Sarrao, J. D. Thompson, Z. Fisk, and P. Monthoux, J. Phys.: Condens. Matter **13**, L337 (2001).

[6] J. D. Thompson *et al.*, J. Magn. Magn. Mater. **226–230**, 5 (2001).

[7] G. Chen, S. Ohara, M. Hedo, Y. Uwatoko, K. Saito, M. Sorai, and I. Sakamoto, J. Phys. Soc. Jpn. **71**, 2836 (2002).

[8] J. L. Sarrao, L. A. Morales, J. D. Thompson, B. L. Scott, G. R. Stewart, F. Wastin, J. Rebizant, P. Boulet, E. Colineau, and G. H. Lander, Nature (London) **420**, 297 (2002).

[9] E. D. Bauer *et al.*, Phys. Rev. Lett. **93**, 147005 (2004).

[10] N. J. Curro, T. Caldwell, E. D. Bauer, L. A. Morales, M. J. Graf, Y. Bang, A. V. Balatsky, J. D. Thompson, and J. L. Sarrao, Nature (London) **434**, 622 (2005).
[11] E. G. Moshopoulou, Z. Fisk, J. L. Sarrao, and J. D. Thompson, J. Solid State Chem. **158**, 25 (2001).
[12] P. G. Pagliuso, C. Petrovic, R. Movshovich, D. Hall, M. F. Hundley, J. L. Sarrao, J. D. Thompson, and Z. Fisk, Phys. Rev. B **64**, 100503(R) (2001).
[13] P. G. Pagliuso, R. Movshovich, A. D. Bianchi, M. Nicklas, J. D. Thompson, M. F. Hundley, J. L. Sarrao, and Z. Fisk, Physica B **312–313**, 129 (2002).
[14] N. D. Mathur, F. M. Grosche, S. R. Julian, I. R. Walker, D. M. Freye, R. K. W. Haselwimmer, and G. G. Lonzarich, Nature (London) **394**, 39 (1998).
[15] T. Takeuchi, T. Inoue, K. Sugiyama, D. Aoki, Y. Tokiwa, Y. Haga, K. Kindo, and Y. Onuki, J. Phys. Soc. Jpn. **70**, 877 (2001).
[16] U. Alver *et al.*, Phys. Rev. B **64**, 180402(R) (2001).
[17] V. F. Correa, L. Tung, S. M. Hollen, P. G. Pagliuso, N. O. Moreno, J. C. Lashley, J. L. Sarrao, and A. H. Lacerda, Phys. Rev. B **69**, 174424 (2004).
[18] P. G. Pagliuso, J. D. Thompson, M. F. Hundley, J. L. Sarrao, and Z. Fisk, Phys. Rev. B **63**, 054426 (2001).
[19] P. G. Pagliuso, J. D. Thompson, M. F. Hundley, and J. L. Sarrao, Phys. Rev. B **62**, 12266 (2000).
[20] E. Granado, P. G. Pagliuso, C. Giles, R. Lora-Serrano, F. Yokaichiya, and J. L. Sarrao, Phys. Rev. B **69**, 144411 (2004).
[21] E. Granado, B. Uchoa, R. Lora-Serrano, A. Malachias, H. Westfahl, Jr., and P. G. Pagliuso, Phys Rev. B (to be published).
[22] Wei Bao, P. G. Pagliuso, J. L. Sarrao, J. D. Thompson, Z. Fisk, J. W. Lynn, and R. W. Erwin, Phys. Rev. B **62**, R14621 (2000); **63**, 219901(E) (2001).
[23] W. Bao, P. G. Pagliuso, J. L. Sarrao, J. D. Thompson, Z. Fisk, and J. W. Lynn, Phys. Rev. B **64**, 020401(R) (2001).
[24] S. Chang, P. G. Pagliuso, W. Bao, J. S. Gardner, I. P. Swainson, J. L. Sarrao, and H. Nakotte, Phys. Rev. B **66**, 132417 (2002).
[25] R. Lora-Serrano, L. M. Ferreira, D. J. Garcia, E. Miranda, C. Giles, J. G. S. Duque, E. Granado, and P. G. Pagliuso, Physica B **384**, 326 (2006).
[26] P. G. Pagliuso *et al.*, J. Appl. Phys. **99**, 08P703 (2006).
[27] C. Giles, F. Yokaichiya, S. W. Kycia, L. C. Sampaio, D. C. Ardiles-Saravia, M. K. K. Franco, and R. T. Neuenschwander, J. Synchrotron Radiat. **10**, 430 (2003).
[28] J. P. Hill and D. F. McMorrow, Acta Crystallogr., Sect. A: Found. Crystallogr. **52**, 236 (1996).
[29] J. A. Blanco, D. Gignoux, and D. Schmitt, Z. Phys. B: Condens. Matter **89**, 343 (1992).
[30] J. A. Blanco, D. Gignoux, and D. Schmitt, Phys. Rev. B **45**, 2529(R) (1992).
[31] A. R. Ball, D. Gignoux, D. Schmitt, and F. Y. Zhang, Phys. Rev. B **47**, 11887 (1993).
[32] S. W. Lovesey and S. P. Collings, *X-Ray Scattering and Absorption by Magnetic Materials* (Oxford Science, Oxford, 1996).
[33] C. Detlefs, A. H. M. Z. Islam, A. I. Goldman, C. Stassis, P. C. Canfield, J. P. Hill, and D. Gibbs, Phys. Rev. B **55**, R680 (1997).
[34] G. Evans and R. F. Pettifer, J. Appl. Crystallogr. **34**, 82 (2001).
[35] M. van Veenendaal, J. B. Goedkoop, and B. T. Thole, Phys. Rev. Lett. **78**, 1162 (1997).
[36] D. F. McMorrow, D. Gibbs, and J. Bohr, in *Handbook on the Physics and Chemistry of Rare Earths*, edited by K. A. Gshneidner Jr. and L. Eyring (North-Holland, Amsterdam, 1997).
[37] J. W. Kim, Y. Lee, D. Wermeille, B. Sieve, L. Tan, S. L. Bud'ko, S. Law, P. C. Canfield, B. N. Harmon, and A. I. Goldman, Phys. Rev. B **72**, 064403 (2005).
[38] H. Stragier, J. O. Cross, J. J. Rehr, L. B. Sorensen, C. E. Bouldin, and J. C. Woicik, Phys. Rev. Lett. **69**, 3064 (1992).
[39] J. P. Hannon, G. T. Trammell, M. Blume, and D. Gibbs, Phys. Rev. Lett. **61**, 1245 (1988).